Journal of the Korean Physical Society, Vol. 48, No. 1, January 2006, pp. 67∼74

Characteristics of a Microwave Plasma Torch with a Coaxial Field-Structure at Atmospheric Pressure

Young S. Bae,* Woo C. Lee, Kyung B. Ko, Yong H. Lee, Won Namkung and Moo H. Cho
Pohang University of Science and Technology, Pohang 790-784

(Received 17 February 2005)

An atmospheric microwave plasma torch is developed using a DC magnetron at 2.45 GHz. We introduce a waveguide-based coaxial field-structure in the plasma torch region, which consists of a waveguide hole boundary in the wide wall (H-plane) of a tapered and shorted WR-284 waveguide. The nozzle penetrates perpendicularly through the H-planes with its tip aligned at the outer plane. The flame-like plasma is formed above the nozzle according to the electric-field distribution radiated from the waveguide hole. The plasma flame appears to be the same as the flame of a burnable gas torch with high gas flow rate; the flame melts molybdenum easily with an average microwave power of 200 W and 5.0-liter per minute (*lpm*) air flow. The spectroscopic measurement for the gas temperature verified that the plasma flames are in the proximity of local thermodynamic equilibrium (LTE) based on the Griem criterion. An ion drift is also seen to exist in the plasma flame from the single Langmuir probe measurement. This plasma torch system is also applied to the treatment of benzene, a volatile organic compound. From the experimental results, 98 % of a high level of 900-ppm benzene is removed easily with an average microwave power of 250 W. For good microwave power coupling into the plasma flame, the hole diameter and the nozzle size are determined by using high frequency structure simulator (HFSS) program.

PACS numbers: 52.75.H, 52.50.D
Keywords: Microwave plasma, Atmospheric pressure, Decomposition

I. INTRODUCTION

Environmental awareness has motivated research and development of the microwave plasma-torch system at atmosphere pressure. The early work was performed for the treatment of toxic gas streams from mobile emitting sources, such as NO_x, SO_x, and of soot emission from diesel engines [1,2]. In particular, the atmospheric waveguide-based microwave plasma-torch can be used to decompose toxic gases such as fluorocarbons and VOCs (volatile organic compounds). The CF_4 of fluorocarbon gas is used in the etching process of semiconductor manufacturing processes. VOCs are widely used as ingredients in household products. Paints, varnishes, and wax all contain organic solvents. All of these products can release organic compounds while you are using them, and, to some degree, when they are stored. They are relatively insignificant as direct greenhouse gases. Instead, they act indirectly by producing organic aerosols in the atmosphere, like ozone, which themselves are direct greenhouse gases. Fluorocarbons or VOCs are known to be difficult to decompose by using conventional arc plasmas with a electrode systems. However, it was reported that CF_4 could be easily decomposed using a microwave torch plasma [3,4]. The decomposition of VOCs is illustrated in this paper by using benzene. The plasma conditions of high temperatures, high degrees of dissociation, and substantial degrees of ionization can be used to accelerate thermodynamically favorable chemical reactions without a catalyst or to provide the energy required for endothermic reforming processes.

The microwave plasma-torch system in Refs. 3 and 5 used a quartz tube penetrating through the center of the larger waveguide walls, inside of which the plasma flame was confined. An igniter was inserted into the quartz tube to ignite the plasma. In this system, the swirl gas entered the discharge tube sideways, creating a vortex flow in tube and stabilizing the torch flame in the center tube [6]. An other type of microwave plasma-torch device, the TIAGO (Torche à Injection Axiale sur Guide d'Ondes, in French) design, is presented in Ref. 7. It has a coaxial field-structure. Such structures first appeared in the 1950s and the 1960s [8–11]. The microwave transmits into the coaxial region, composed of the waveguide hole boundary and the nozzle, where the plasma flame can be generated. The TIAGO design is a modified version of the TIA (Torche à Injection Axiale, in French) design, which has many shortcomings [12]. The TIAGO design eliminates the shortcomings, and it has a one-nozzle unit whose tip is located at higher level than the

*E-mail: ysbae7@postech.ac.kr; Fax: +82-54-279-1299

outer plane, providing a single plasma flame. The plasma is sustained by 2.45-GHz microwaves in a stream of gas surrounded by air at the tip of the nozzle. Gas feeding occurs axially through the nozzle.

The device described in this paper has a coaxial field-structure, which is similar to the TIAGO design. However, the nozzles of the microwave torch system are designed in order to feed two different gases. In addition, the nozzle tip is aligned to the outer plane. A stable plasma jet can be sustained with a high flow rate of air or argon gas and with low microwave power reflection. The impedance is matched using a three-stub tuner and a movable short. The optimum design of the coaxial torch region is obtained by using the HFSS (high-frequency structure simulator) program [13], and the design was verified experimentally. The overall system design is described, and experimental torch performance characteristics are explored in the following sections. The design of the plasma torch is described in Section II. The experiments and the results for the characteristics of the torch system are described in Section III. The removal experiments on high levels of benzene are discussed in Section IV, which is followed by conclusions in Section V.

II. DESIGN OF THE PLASMA TORCH

The waveguide used in this system is the standard WR284 waveguide, which has rectangular inner dimensions of width $a = 7.2$ cm and height $b = 3.4$ cm. The E-plane is reduced by half in order to get a plasma with a lower microwave power consumption. The end of the waveguide line is shorted, and a nozzle is positioned with an offset from the shorted end. The offset is adjusted by using a movable, sliding short line connected at the end. Figure 1 shows a schematic of the torch system. The 2.45-GHz microwaves are generated from a DC magnetron. The DC magnetron generates a maximum 1.5 kW of microwave power. A circulator and a dummy load are used to protect the magnetron from the microwaves reflected from the plasma torch region. The reflected microwaves are absorbed in the dummy load attached to an isolator. The incident and reflected powers are monitored by using the directional couplers D/C 1 and D/C 2 shown in Figure 1. The reflection power is minimized using a 3-stub tuner installed after the directional coupler.

If a plasma is to be obtained with a lower power consumption, the height b of the waveguide must be reduced to $b/2$ before the torch region. The reducing of the height gives us an increases in the electric field strength even with the same microwave power. The power transferred in the WR284 waveguide is calculated from the Poynting theorem. Before the E-plane taper,

$$P_1 = \frac{1}{2}\mathrm{Re}\int_0^a \int_0^b -E_y H_x^* dxdy. \quad (1)$$

After the E-plane taper,

$$P_2 = \frac{1}{2}\mathrm{Re}\int_0^a \int_0^{b/2} -E_y H_x^* dxdy. \quad (2)$$

E_0 and E_0' are the maximum electric field strengths in the waveguide before and after the taper, respectively. Since the fundamental wave propagation mode, the TE_{10}-mode, does not depend on the b dimension, Eqs. (1) and (2) are then

$$P_1 = \frac{E_0^2 ba}{4Z_{\mathrm{TE}}}, \quad (3)$$

$$P_2 = \frac{E_0^{'2}(b/2)a}{4Z_{\mathrm{TE}}}, \quad (4)$$

where Z_{TE} is the characteristic waveguide impedance given by

$$Z_{\mathrm{TE}} = \sqrt{\frac{\mu_0}{\epsilon_0}}\left[1-\left(\frac{\lambda}{2a}\right)^2\right]^{-1/2}, \quad (5)$$

where λ being the free-space wavelength. From Eqs. (3) and (4) with $P_1 = P_2$,

$$E_0' = \sqrt{2}E_0. \quad (6)$$

Therefore, we get about a 1.4 times higher electric field strength in the torch region.

The optimum length of the E-plane taper for the low reflection is determined using the HFSS program. The taper can be designed by using two methods: (a) tapering both sides of the E-planes simultaneously or (b) tapering only one side of the E-planes. The taper can be considered as a two-port network device. The HFSS simulation gives the S-parameters as a function of frequency. Figure 2 shows the reflection (20 log S11) as a function of the frequency for the above two cases. There is no difference between the two cases for a taper length of λ_G. In addition, the reflection is less than 30 dB. Where λ_G is the guided wavelength (23.2 cm) for a frequency of 2.45 GHz in the WR284 waveguide. An E-plane taper of type-(b) was selected because of easy fabrication.

The torch structure is a coaxial-field structure. It consists of a waveguide hole boundary in the H-plane and

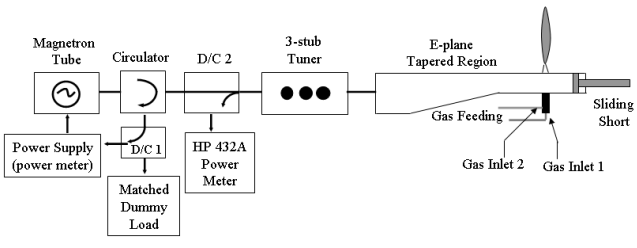

Fig. 1. Schematic diagram of the experimental setup.

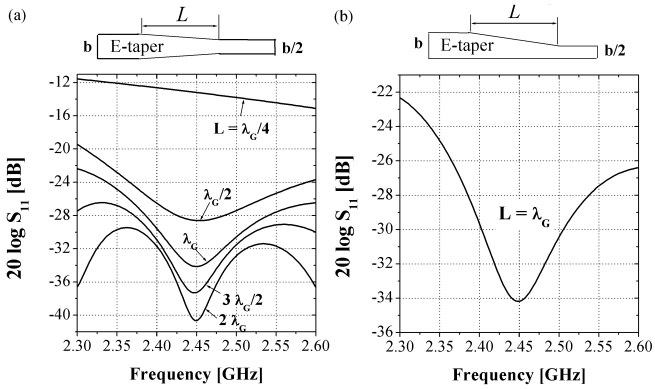

Fig. 2. Reflection of two kinds of tapers as functions of the frequency for various taper lengths.

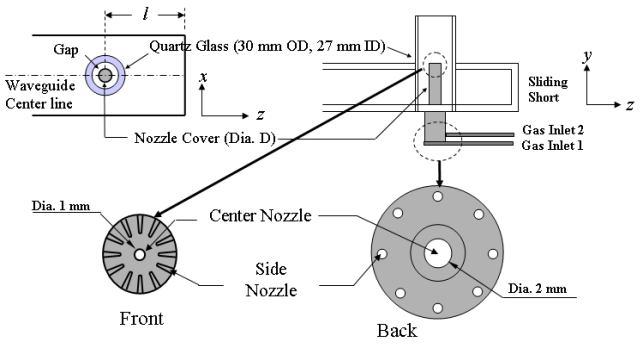

Fig. 3. Schematic drawing of the coaxial-field structure of the torch system.

a nozzle. The nozzle penetrates into the waveguide perpendicular to the H-plane, and its tip is aligned at the outer plane. The detailed torch structure is shown in Figure 3. The quartz tube is inserted in order to confine the plasma flame in the free-bounded space. Two different gases can be fed through the center nozzle and the side nozzle coaxially. The diameter of the center nozzle is tapered from the bottom to the tip. The side nozzle is set to assist with the stability of the plasma-flame flowing argon gas.

The diameters of the waveguide hole boundary and the nozzle for good microwave coupling into the plasma are found by using the HFSS program. The model of the torch region used in the HFSS simulation is shown in Figure 4. The plasma flame is modelled as water in a cylindrical shape with a 0.5-cm diameter and a 3-cm height because the most microwave power can be absorbed in the plasma in the ignition phase. After ignition, the most incident microwave power consumption can be thought to occur on the plasma flame surface because the microwaves cannot penetrate the plasma due to the high plasma density. In the experiment, the flame length increases with increasing incident microwave power. Therefore, the plasma flame might be considered as cylindrical metal. However, in this simulation, the water modelling of the plasma flame is valid

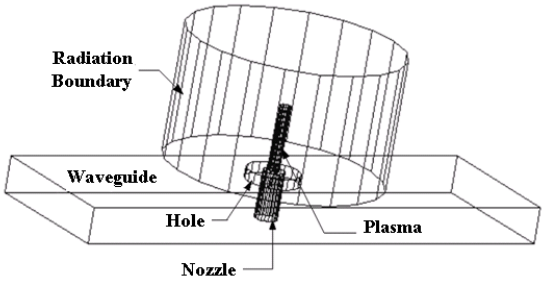

Fig. 4. HFSS model for calculating the absorbed power and the radiated power in the torch region.

if only the ignition phase is considered. The material properties of the plasma flame are set to those of water; that is, the dielectric constant is 81, and the loss tangent is 0.205. The radiation boundary is modelled as a cylinder box with a 10-cm diameter and a 6-cm height that completely absorbs any microwave power incident on its boundaries.

We compared the radiated power with the power absorbed in the plasma (the water in the model) for various hole diameters and a nozzle length of 2.2 cm. This nozzle length aligns the top of the nozzle with the outer plane of the H-plane. The radiated power and the absorbed power are integrated over the radiation boundary surfaces of the cylinder and over the plasma volume, respectively:

$$P_{rad} = \frac{1}{2\mu_0}\mathrm{Re}\int |\vec{E}\times\vec{B}^*|dS_{\mathrm{rad}}, \tag{7}$$

$$P_{abs} = \frac{1}{2}\mathrm{Re}\int |\vec{J}^*\cdot\vec{E}|dV_{\mathrm{plasma}}, \tag{8}$$

where $\vec{E}$ is the electric field, $\vec{B}$ is the magnetic field, $\vec{J}$ is the displacement current in volume, dS_{rad} is an infinitesimal surface of the radiation boundary, and dV_{plasma} is an infinitesimal plasma volume.

Figure 5 (a) shows plots of the absorbed power and its ratio to the radiated power, as calculated by using the HFSS simulation. The absorbed power increases as the hole-diameter increases, but its ratio decreases. When the hole-diameter is 2 cm or 2.5 cm, the plasma is observed to exist only in the gap region. Even with the proper gas flow, the plasma cannot grow upright to form a flame-like shape. With a larger hole-diameter, there is higher radiated power: this is not desirable situation. Therefore, a 3-cm hole diameter was chosen for the torch performance experiments. This hole diameter was obtained for an optimum nozzle outer diameter of 1 cm. We also investigated the effect of the nozzle length, as shown in Figure 5 (b). When the nozzle juts out from the hole plane, the absorption efficiency decreases. However, when the nozzle is below the hole plane, the plasma flame becomes unstable when the gas flows, and it is rather difficult to get an upright stable plasma flame. Therefore, a

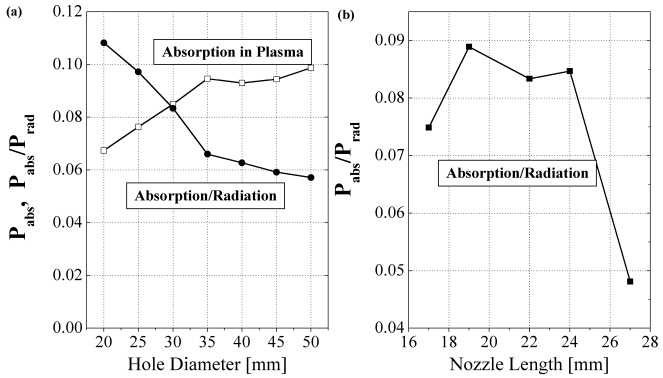

Fig. 5. (a) Absorbed power in the plasma and its ratio to the radiated power as functions of the hole diameter, and (b) the ratio of the absorbed power to the radiated power as a function of the nozzle length. In (a), the scale of the ratio of the absorbed power to the radiated power is adjusted to be compared with the power absorbed in the plasma.

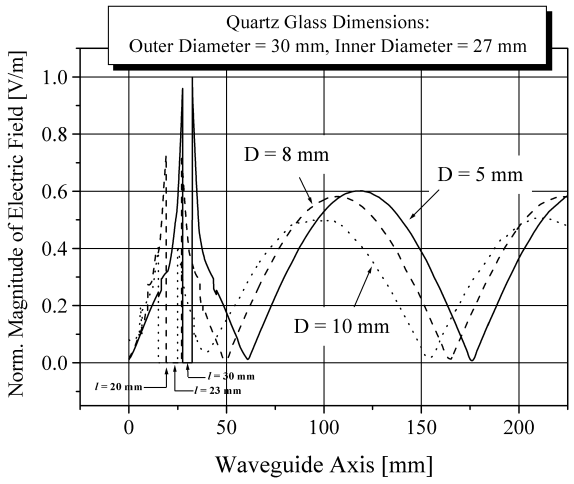

Fig. 6. Normalized magnitudes of the electric field on the waveguide axis, the waveguide-center line in the parallel direction to the propagating wave, for various nozzle diameters.

hole of 3 cm diameter was made on the centerline of the H-plane, and the nozzle tip was aligned with the outer plane of the waveguide's H-plane. The position of the waveguide shorting-plate from the nozzle was determined so as to have the electric fields distributed symmetrically from the center of the nozzle by using the HFSS program.

From the HFSS simulation, the shorting-plate position is seen to depend on the nozzle-cover diameter (D), as shown in Figure 6. Since the nozzle-cover diameter is 0.8 cm, the shorting-plate should be positioned 2.3 cm away from the center of the nozzle for a symmetric distribution of the electric fields. For a 0.8-cm nozzle-cover diameter and a 2.3-cm shorting-plate position, the electric field configurations are also plotted in all regions of the HFSS model. Figure 7 shows that the electric field lines are shaped between the nozzle and the boundary of the hole. Therefore, the plasma should be initiated in

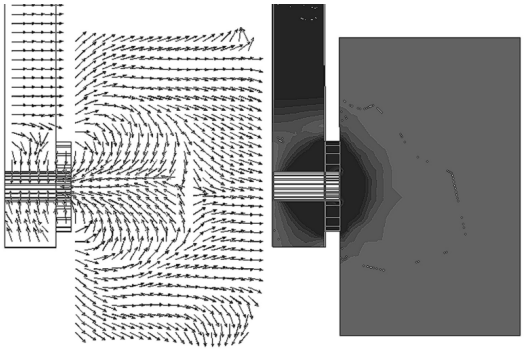

Fig. 7. (Left)Distribution of the electric field lines and (right) the contour plot of the electric field in the waveguide and the radiation region

the gap around the nozzle.

III. CHARACTERISTICS OF THE PLASMA TORCH

A high breakdown voltage is required to initiate the plasma discharge at atmospheric pressure. It is difficult to supply such a high breakdown voltage just by using microwave power. Thus, we need a system to ignite a spark between the two electrodes. This requires another power supply. A simple method to make an ignition spark is just to touch the nozzle tip using a piece of metal, *i.e.*, electrical shorting of two electrodes. In our experiment, we investigated the microwave power reflection as a function of the gas flow rate for various incident microwave powers. Air and argon gases are used for this experiment. The gas flow rates at the center nozzle and the side nozzle are controlled independently using gas flow controllers. In the practical application, one can feed the toxic gases into the center nozzle and the other buffer gases, such as plasma stabilizing gases and chemical additives, through the side nozzle. In this experiment, the air is fed through the center nozzle, and the argon gas is fed through the side nozzle. We first wanted to seek the optimum position of the shorting plate. We applied an incident microwave power of 300 W and fed air at a 5-*lpm* flow rate. The 3-stub tuner was adjusted to have a low microwave power reflection with the proper shorting-plate position. Then, we measured the microwave power reflection while changing the position of the shorting plate. Figure 8 shows the measurement results. Minimum microwave reflection was achieved with a shorting-plate position in the range of 2 cm to 2.5 cm.

For all other experiments, the shorting plate was positioned 2.5 cm away from the nozzle. Figure 9 shows the dependence of the microwave power reflection on the air flow rate of the center nozzle without side gas feeding. For an incident microwave power of 500 W, we obtain

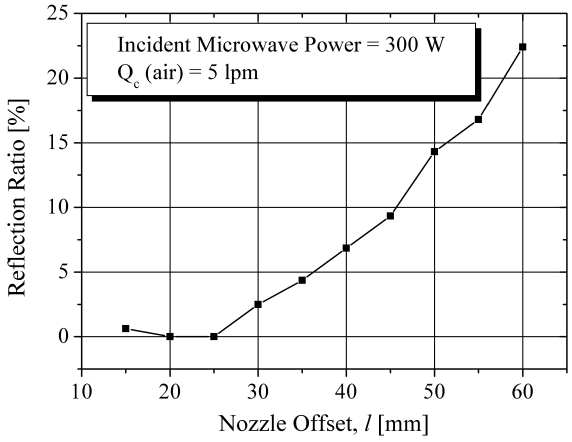

Fig. 8. Reflection ratio as a function of the shorting-plate position. The incident microwave power is 300 W, and the air gas flow rate is 5 *lpm*.

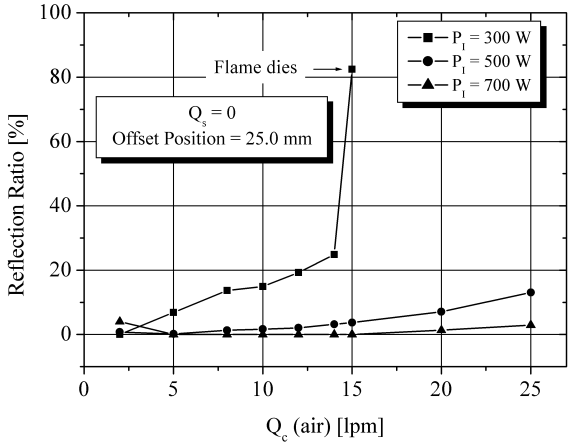

Fig. 9. Dependence of microwave power reflection on the air flow rate of the center nozzle without side gas feeding.

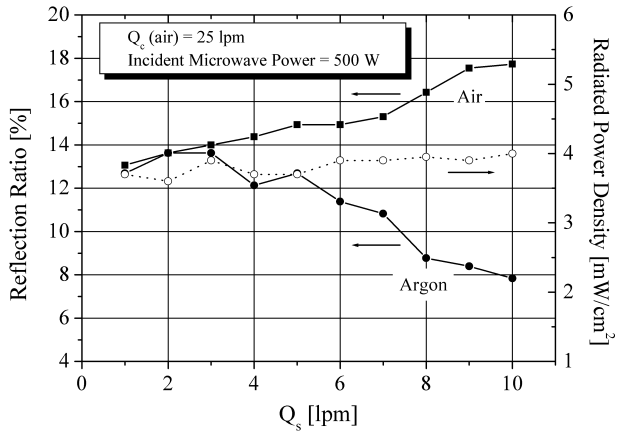

Fig. 10. The effect of the side gas flow rate on the power reflection and the radiated power density. The incident microwave power is 500 W, and the air gas flow rate of the center nozzle is 25 *lpm*. The radiated power density is measured for the argon gas.

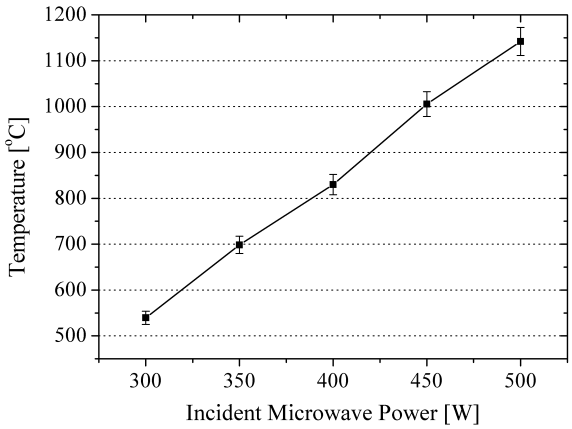

Fig. 11. Temperature at 10 cm from the nozzle, as measured using a B-type thermocouple, as a function of the incident microwave power. The argon gas flow rate is fixed at 4 *lpm*.

a microwave power reflection of less than 15 % at an air flow rate of 25 *lpm*. The microwave power reflection rate starts to increase rapidly after 12 *lpm*, but at higher incident microwave powers, the reflection rate becomes lower. Figure 10 shows the effect of the side gas flow rate. The incident microwave power is 500 W and the air is flowing into the center nozzle at a flow rate of 25 *lpm*. When we feed air into the side nozzle and the center nozzle simultaneously, the reflection increases as the flow rate at the side nozzle increases. Increasing the gas flow rate by 10 *lpm* at the side nozzle increased the reflection ratio by 5 %. When we increased air flow by 10 *lpm* at the center nozzle, not the side nozzle, the reflection was larger than 5 %. This can be explained by the swirling effect of the side nozzle. When air was replaced by argon gas, the reflection ratio decreased. Argon gas seemed to assist in microwave power absorption because of the little change in the radiated power density as shown in Figure 10. The radiated power density was measured at the maximum radiation point by using a microwave survey meter calibrated at 2.45 GHz.

The change in the torch length with the microwave power was observed from the temperature measurement near the end of the torch flame. Figure 11 shows the temperature measured near the end of the torch flame by using a B-type TC (thermocouple) fixed at about 10 cm above the nozzle tip. The torch flame rises up with an incident microwave power of 500 W and the argon gas flow rate of 4 *lpm*. When the microwave power is reduced, the torch length becomes shorter; hence, the temperature decreases as shown in Figure 11. Figure 12 shows the plasma-torch flames without the quartz tube for various gas flow rates. They look more like burnable gas torch flames as the gas flow rate is increased for a fixed incident microwave power. From the experiments, the quartz tube is understood to confine the ions emerging from the plasma flames. When the quartz tube is

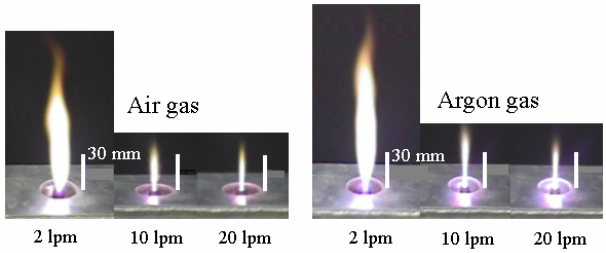

Fig. 12. Air and argon torches are compared for various flow rates for an incident microwave power of 500 W. Rulers of 30 mm are shown at the right side of each torch figure.

Fig. 13. Torch-flame and background plasma inside the quartz tube.

inserted, a background plasma is seen around the top of the flame inside the quartz (see Figure 13).

The proximity to LTE of plasma flames is verified from Griem criterion [14] and Timofeev's electron density expression [15]. The Griem criterion states the threshold electron density for the LTE condition and is given by

$$n_e \geq 9 \times 10^{11} \left(\frac{\Delta E}{E_H}\right)^3 \sqrt{\frac{T_e}{E_H}}, \qquad (9)$$

where n_e is the electron density in cm^{-3}, ΔE is the energy level difference between the ground state and the first ionization state, E_H is the ionization potential for hydrogen (13.6 eV), and T_e is the electron temperature. Evaluating Eq. (9) for an electron temperature of approximately 1 eV and for a ΔE corresponding to the ionization potential for the N_2 molecule (15.6 eV) results in an electron density threshold of $\sim 3 \times 10^{11}$ cm^{-3} for LTE.

Timofeev developed an electron density expression based on experimental data from an atmospheric pressure spherically symmetric microwave air discharge. The electron density is given by

$$n_e = \begin{cases} 5.91 \times 10^{15} \exp\left[-\frac{14.42}{T-1.74}\right] & (T > 1.74) \\ 0 & (T < 1.74), \end{cases} \qquad (10)$$

where n_e is in cm^{-3} and T is the gas temperature at

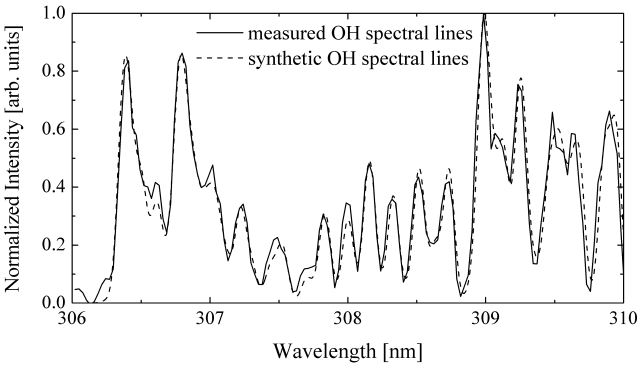

Fig. 14. The measured OH spectrum (solid line) and the synthetic OH spectrum for the rotational temperature of 4500 K (dashed line).

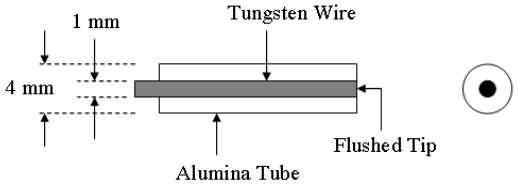

Fig. 15. Geometry of the single Langmuir probe.

LTE measured in 10^3 K. Here, the rotational temperature of the OH molecule is used for the gas temperature, which determined from a spectroscopic measurement of the OH molecule's spectra [16]. The rotational temperature is simply obtained by comparing the synthetic spectrum with the measured spectrum by using the chi-square method. For the spectroscopic measurement, the fiber optic is connected to an 0.75 m-spectrometer which has a 1200-groove/mm grating, an adjustable slit, and a charge coupled device (CCD) detector array with 1024 by 128 pixels. For the measurements with the OH atomic emission lines, the spectrometer is tuned to cover the 306 - 310-nm spectral range with a spectral resolution of about 0.025 nm. Figure 14 shows an obtained OH spectrum for an average microwave power of 400 W and a 1-*lpm* Ar gas flow. From the synthetic spectrum, the rotational temperature is about 4500 K. This temperature gives us an n_e of $\sim 1 \times 10^{13}$ cm^{-3}. This value is much higher than the threshold electron density given by Eq. (9).

The plasma parameters in the edge layer of the plasma flame are investigated using a single Langmuir probe [17]. The Langmuir probe is constructed from tungsten wire with a diameter equal to 1 mm. A schematic of the probe is shown in Figure 15. The tungsten wire is inserted into an alumina tube with an outer diameter equal to 4 mm. A planar-type probe tip is obtained by flushing the tungsten wire at the end of the alumina tube. The Langmuir probe is scanned in the axial direction of the gas flow around the edge layer of the plasma flame. Figure 16 shows two I-V traces; the solid line is one mea-

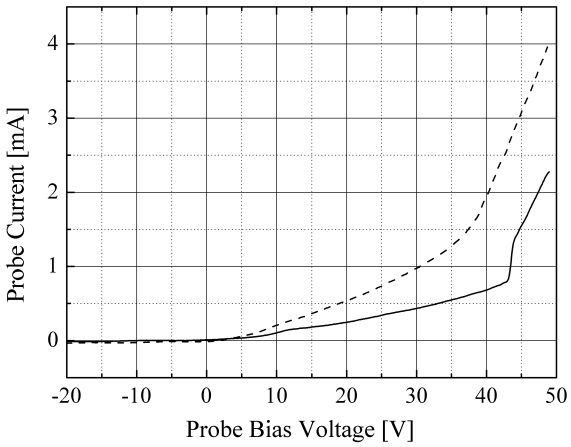

Fig. 16. I-V traces measured at two different positions.

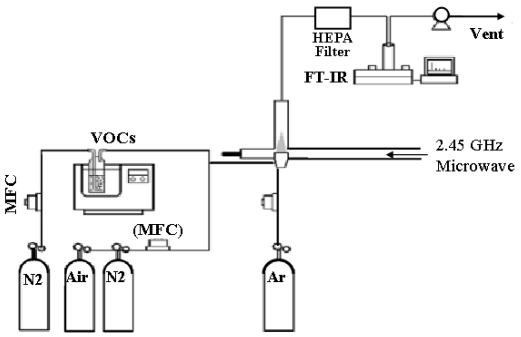

Fig. 17. Schematic layout of the benzene-removal experimental setup.

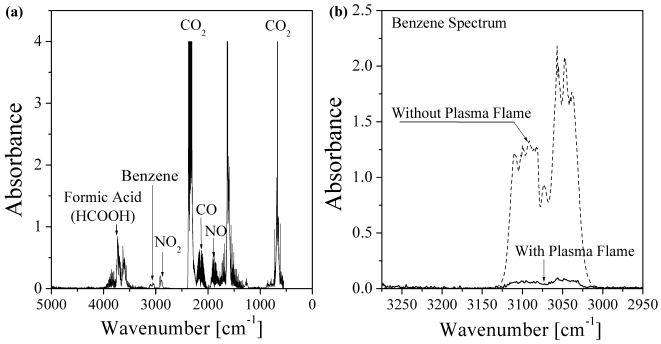

Fig. 18. (a) Measured FT-IR molecular spectra of a mixed gas after passing through the plasma flame. Here, the microwave power is 200 W. (b) Magnified view of the benzene peaks with and without a plasma flame. Benzene is removed significantly by the plasma flame. Here, the microwave power is 500 W.

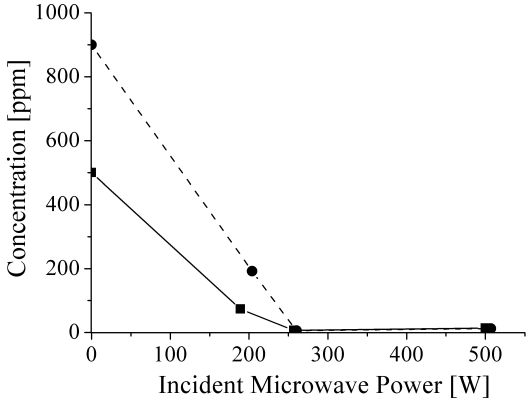

Fig. 19. Removal characteristics of high levels of benzene as a function of the incident microwave power.

sured far from the core plasma, and the dashed line is one measured close to the core plasma. Even though the theory of the Langmuir probe (LP) for an atmospheric plasma has not been studied, these I-V traces seem to show that the plasma flame in the outer region is a drifting Maxwellian plasma with beam ions with energies of $E_{bi} = 40$ V and with very small temperature compared to the electron temperature, according to the collisionless LP theory [18]. We see a gentle slope at a bias voltage of 40 V in the dashed I-V trace in Figure 16 because the ion temperature near the core is higher than at the edge.

IV. BENZENE-REMOVAL EXPERIMENT

Benzene is an aromatic hydrocarbon that is produced by the burning of natural products. It is a component of products derived from coal and petroleum and is found in gasoline and other fuels. Benzene is used in the manufacture of plastics, detergents, pesticides, and other chemicals. Research has shown benzene to be a carcinogen (cancer causing). With exposures from less than five years to more than 30 years, individuals have developed, and died from, leukemia. Long-term exposure may affect bone marrow and blood production. Short-term exposure to high levels of benzene can cause drowsiness, dizziness, unconsciousness, and death.

The microwave plasma-torch system described in the previous sections can be applied to the benzene-removal experiment. Figure 17 shows the experimental layout for benzene-removal. The removal efficiency is measured using a FT-IR (Fourier transform infra-red) spectrometer (ABB Bomem Inc., MB 104). The Fourier-transformed peak signal of benzene is in the range of $k = 3000 \sim 3200$ cm^{-1}, where k is the wavenumber. The molecular spectra measured by FT-IR spectroscopy is identified by means of comparing their wavenumbers and shapes with those of measured spectral data with known molecules.

A mixed gas of benzene to be decomposed, argon gas, and air was used for this experiment. Figure 18 (a) shows the FT-IR spectra of the various molecules contained in the gas after it had been passed through the plasma flame, which had been produced by a microwave power of 200 W. Carbon dioxide (CO_2), carbon monoxide (CO), nitrogen dioxide (NO_2), and nitric oxide (NO) peaks appear in the spectrum. CO and CO_2 products come from reactions between the oxygen contained in air and the

carbon contained in benzene. NO and NO_2 come from the thermal NOx produced by the thermal plasma. Figure 18 (b) shows a magnified view of the benzene peaks. A significant removal of the benzene is seen from a comparison of the benzene peaks with and without a plasma flame at a microwave power of 500 W. The concentration of benzene is controlled by the flow rate of the nitrogen carrier gas. In the removal experiment, argon gas and benzene with nitrogen gas are fed into the center nozzle and the side nozzle, respectively. Both the flow rates of the argon and the nitrogen gases are 2 *lpm*. Figure 19 shows the removed amounts of high levels of 500-ppm and 900-ppm benzene as functions of the incident microwave power. The initial levels of 500 ppm and 900 ppm are decreased significantly with increasing incident microwave power. More than 98 % of both benzene levels are removed as the incident microwave power is increased to 250 W.

V. CONCLUSION

An atmospheric waveguide-based plasma torch system is developed by introducing the coaxial field-structure. The optimum dimension of the coaxial structure is determined by the help of the HFSS simulation and confirmed in the experiments. The experiments showed that the coaxial-field structure provides good microwave coupling hence a very stable plasma flame even with the high incident microwave power. The spectroscopic measurements showed that the plasma flame is in the proximity of LTE. The Langmuir probe measurements also showed ion drift in the plasma flame. The gentle slope in I-V trace measured near the core convinces that there exist drifting ions with the higher thermal temperature. The plasma torch is applied to the benzene-removal experiment. In this experiment, more than 98 % of the high level benzene of 900 ppm is removed with an average microwave power of 250 W. The good removal efficiency results from the decomposition of benzene by high gas temperature of the thermal plasma flame. It is expected that this torch system yield a good removal efficiency of even a direct greenhouse gas, such as methane gas. Therefore, more experiments will be done in near future. Also, the characteristics of the plasma parameters, the gas temperature and the plasma density, will be extensively investigated using the spectroscopic method and the Langmuir probe.

ACKNOWLEDGMENTS

The authors are very appreciative for the technical help provided by the members of the Molecular Science and Technology Laboratory at the Ajou University. This work is supported partly by Ministry of Science and Technology in Korea (MOST-Korea), Korea Institute of Environmental Science and Technology (KIEST), and Korea Institute of Machinery & Materials (KIMM).

REFERENCES

[1] H. S. Uhm and S. H. Hong, *1997 IEEE International Conference on Plasma Science* (San Diego, 1997).
[2] Y. C. Hong and H. S. Uhm, 28th *IEEE International Conference on Plasma Science and 13th IEEE International Pulsed Power Conference* (Las Vegas, 2001).
[3] H. S. Uhm: Korea patent 0058109 (2001).
[4] K. M. Green, M.C. Borras, P. P. Woskov, IEEE Trans. Plasma Sci. **29**, 399 (2001).
[5] J. H. Kim, Y. C. Hong, H. S. Kim and H. S. Uhm, J. Korean Phys. Soc. **42**, 876 (2003).
[6] H. S. Uhm, Y. C. Hong and H. J. Kang, US Patent Application **09/880**, 885 (2001).
[7] M. Moisan, Z. Zakrzewski and J. C. Rostaing, Plasma Sources Sci. Technol. **10**, 387 (2001).
[8] J. D. Cobine and D. A. Wilbur, J. Appl. Phys. **22**, 835 (1951).
[9] W. Schmidt, Elektron Rundschau **3**, 404 (1959).
[10] J. Swift, Proc. IREE Australia **25**, 779 (1964).
[11] J. Swift, Electron Eng. **38**, 152 (1966).
[12] M. Moisan, G. Sauve, Z. Zakrzewski and J. Hubert, Plasma Sources Sci. Technol. **3**, 584 (1994).
[13] 3D EM simulation software for RF wireless, packaging and opto-electronic design using a finite element method (FEM), Ansoft Corporation's product, http://www.ansoft.com/.
[14] H. R. Griem, Phys. Rev. **131**, 1170 (1963).
[15] A. V. Timofeev, Plasma Phys. Rep. **23**, No. 72, 158 (1997).
[16] Se Youn Moon and W. Choe, Spectrochimica Acta Part B **58**, 249 (2003).
[17] B. K. Park, G. H. Kim, D. G. Kim and T. Lho, J. Korean Phys. Soc. **42**, S867 (2003).
[18] N. Hershkowitz, *Plasma Diagnostics* edited by O. Auciello and D. L. Flamm (San Diego, CA, 1989), p. 120.